Photon upconversion, structural, and magnetic properties of rare earth-doped $NaYF_4$ nanoparticles

A. F. García-Flores*, G. G. Lesseux**, W. Iwamoto**, R. R. Urbano**, and C. Rettori*,**

* Universidade Federal do ABC, Centro de Ciências Naturais e Humanas,
Santo André-SP, 09210-971, Brazil, agarciaflores1@gmail.com
** Instituto de Física "Gleb Wataghin", UNICAMP, 13083-859
Campinas, São Paulo, Brazil, rettori@ifi.unicamp.br

ABSTRACT

Magnetic, structural, and optical investigations of rare-earths (R) co-doped nanoparticles (NPs) of $NaY_{1-x-y}R^1_xR^2_yF_4$ with $R^1_x = Yb_{0.20}/R^2_y = Er_{0.02}$ and $R^1_x = Yb_{0.30}/R^2_y = Tm_{0.005}$ and single doped (y = 0) with $R^1_x = Yb_{0.20}$ and $R^1_x = Er_{0.02}$ are reported. The visible green and blue upconversion emitted lights of Yb/Er and Yb/Tm co-doped $NaYF_4$ NPs were observed with naked eye and no filters when excited with a 980 nm laser diode. The NPs are mixture of both phases, α (cubic nanospheres: 15-25 nm) and β (hexagonal nanoplates: ∼230 nm). From the observed electron spin resonance (ESR) signals and Curie-Weiss fits of the temperature dependence of the magnetization, we obtained the oxidation states to be trivalent ions, i.e., Yb^{3+} ($4f^{13}$, $J = 7/2$) and Er^{3+} ($4f^{11}$, $J = 15/2$). As expected for NPs with mixture of α- and β-phases, the ESR spectra broaden toward higher magnetic fields due to the anisotropic contribution of the crystal electric field to the Kramer ground state g-values.

Keywords: upconversion, nanoparticles, rare earth, magnetic properties

1 INTRODUCTION

Nowadays, remarkable attention is being given to nanocrystalline materials with upconversion properties due to their technological and biomedical potential applications [1], [2]. The study of this phenomenon have evolved into a broad interdisciplinary field that rapidly extended up to the frontiers of the photochemistry, biophysics, solid state physics, and material science. The transfer of upconverted energy has been widely used to offer highly efficient upconversion materials [3]. Upconversion is the process of converting low-energy excited photons into emission of high-energy photons [3]. The upconversion process is mainly associated with a transition to an excited state, energy transfer, and photon avalanche [3], [4] where all these processes involve a sequential absorption of two or more photons. The majority of materials that are able to perform upconversion involves trivalent rare-earths and the efficiency of such a phenomenon is generally restricted to Er^{3+}, Yb^{3+}, Tm^{3+}, and Ho^{3+} activators. These rare-earth elements are characterized by their multiple metastable states arranged as ladder-like levels, essential to facilitate the sequential photon absorptions and the energy transfer steps [5]. Rare-earth fluorides, particularly $NaYF_4$, are regarded as ideal hosts due to their low energy lattice phonons (requirement for minimizing nonradioactive loss and maximizing radioactive emission) and high photochemical stability [5], [6].

Our interest is focused in $NaYF_4$ NPs doped with rare-earth ions. These NPs exist in two phases: a cubic (α-phase) and a hexagonal (β-phase). The NPs in the α-phase are usually small in size and show poor upconversion emission intensity [6]–[8]. On the other side, the β-phase crystallizes in larger units with less defects and present a more intense upconversion emission[9], [10]. Therefore, the NPs with hexagonal β-phase $NaYF_4$ are considered the most efficient upconverter. Actually, different crystalline structures can significantly influence the optical properties of the NPs. The dependence of the optical properties with the crystallographic morphology may be attributed to different electric crystal fields that surround the trivalent rare-earth ions.

In this work, we present optical, morphological, and magnetic results of synthesized $NaYF_4$ NPs doped with trivalent rare-earth ions, specifically, Yb^{3+}, Er^{3+}, and Tm^{3+}. For the Yb/Er and Yb/Tm co-doped $NaYF_4$ NPs, we observed the upconversion emission in the visible spectral range as reported in the literature [10]–[13]. We have confirmed the incorporation of the trivalent rare-earth dopant ions into the $NaYF_4$ lattice by magnetic characterizations in single doped $NaYF_4$ NPs with Yb and Er.

2 EXPERIMENTAL DETAILS

The rare-earth co-doped $NaYF_4$ NPs were synthesized by the chemical method based on Ref.[14] and Ref.[15] where trifluoroacetates were used as precursors in a solution of oleic acid and octadecene at a reaction temperature of 300 °C. The rare-earth trifluoroacetate precursors were prepared from their corresponding oxides and trifluoroacetic acid [16]. The powder X-ray diffraction (XRD) measurements of the dried powders were carried out in a Phyllips Diffractometer with Cu Kα radiation (λ = 1.5418 Å). The size and morpho-

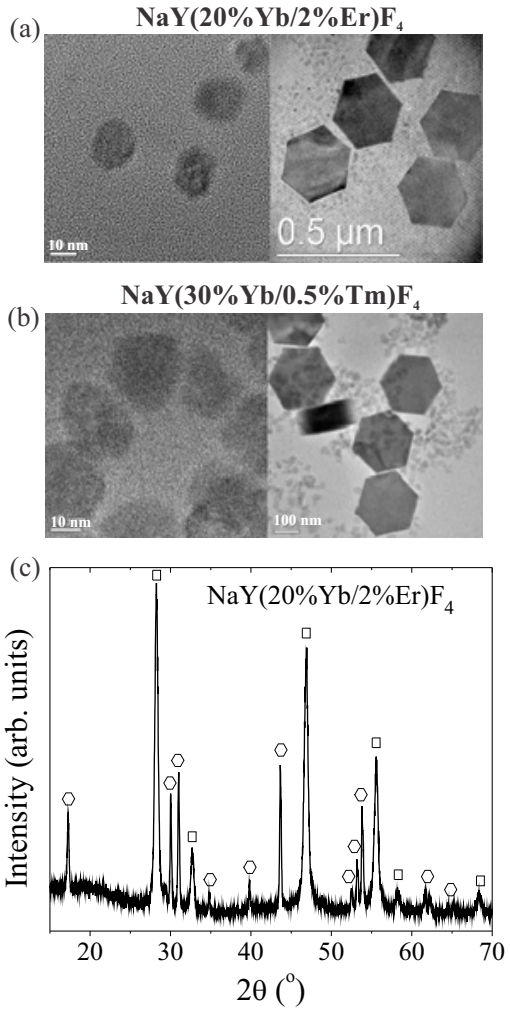

Figure 1: (a) HRTEM images of NaY(20%Yb/2%Er)F_4 and NaY(30%Yb/0.5%Tm)F_4 NPs. (b) XRD patterns of NaY(20%Yb/2%Er)F_4 NPs. The square and hexagonal symbols correspond to the α and β-phases, respectively.

logy of the NPs were characterized by high resolution transmission electron mycroscopy (HRTEM) measurements using a JEOL 3010 transmission electron microscopy operating at an acceleration voltage of 300 kV. The magnetic characterization was performed with a SQUID magnetometer (Quantum Design MPMS) in the T-range of 2-300 K and a applied magnetic field of $H = 2$ KOe. The ESR measurements were carried out in a Bruker-ELEXSYS 500 spectrometer at X-band frequencies ($\nu = 9.48$ GHz) using a TE_{102} resonators coupled to a ^{4}He-flux temperature controller. For the ESR measurements, we used colloidal NPs samples dispersed in toluene. The luminescence measurements were performed using a USB650 Red Tide Spectrometer equipped with a linear silicon CCD array. The luminescence spectra were excited with a 980 nm laser diode with an excitation power density of about 10 W/cm^2.

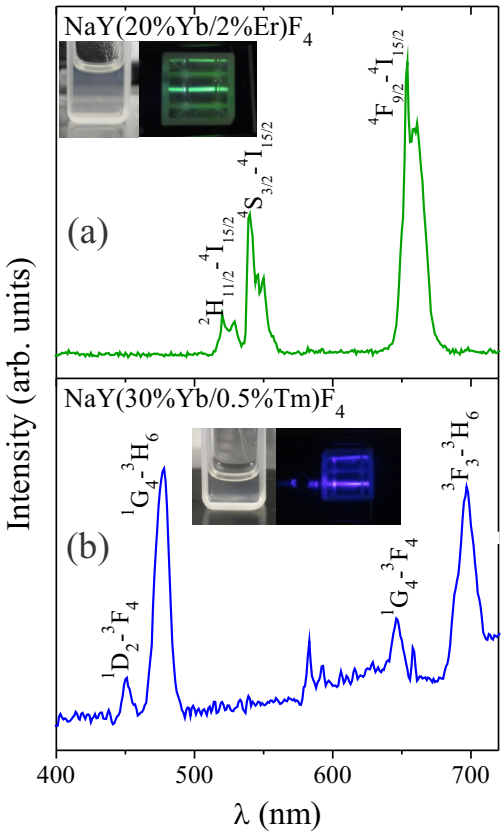

Figure 2: (a) Emission spectra at room-T of NaY(20%Yb/2%Er)F_4 NPs. The observed emission bands correspond to the transitions $^2H_{11/2}$ (∼520 nm), $^4S_{3/2}$ (∼550 nm), and $^4F_{9/2}$ (∼670 nm) (b) Emission spectra at room-T of NaY(30%Yb/0.5%Tm)F_4 NPs. The observed emission bands correspond to the transitions $^1D_2$-$^3F_4$ (∼451 nm), $^1G_4$-$^3H_6$ (∼477 nm), $^1G_4$-$^3F_4$ (∼647 nm), and $^3F_3$-$^3H_6$ (∼697 nm). The insets show their respective digital photographs.

3 EXPERIMENTAL RESULTS AND DISCUSSIONS

Figures 1(a) and 1(b) show the HRTEM images of the Yb/Er and Yb/Tm co-doped $NaYF_4$ NPs. These images clearly indicate the mixture of two crystallographic phases, a roughly spherical cubic nanoparticles and another well defined hexagonal nanoplates. Figures 1(a) and 1(b) reveal that the NPs in the cubic phase vary their size from 15 to 25 nm and the hexagonal nanoplates vary the side-to-side length roughly 230 nm. The XRD patterns of Fig. 1(c) for the Yb/Er co-doped $NaYF_4$ NPs, also confirms the existence of two phases in the synthesized NPs. The well-defined XRD peak positions match closely with the obtained pattern for α-phase (cubic) and β-phase (hexagonal nanoplates) [15]. Figure 2 shows the upconversion emission spectra of NaY(20%Yb/2%Er)F_4 and NaY(30%Yb/0.5%Tm)F_4 NPs for an excitation light

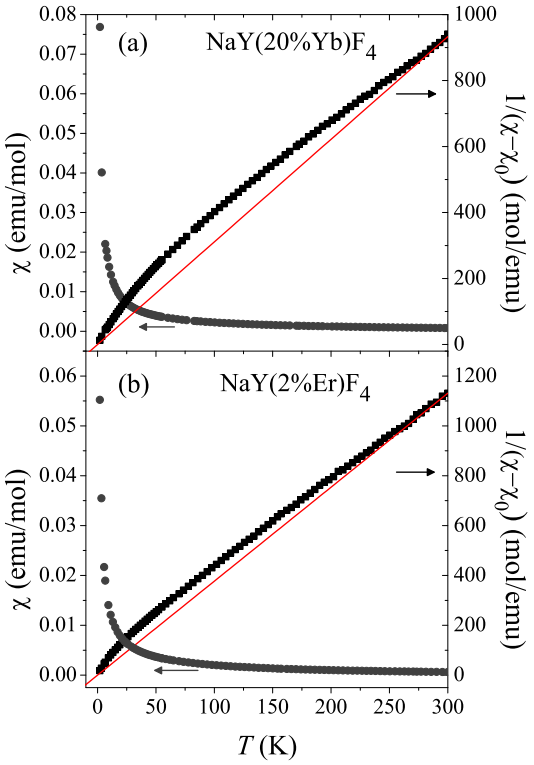

Figure 3: T-dependence of the dc magnetic susceptibility its respective inverse of (a) $NaY(20\%Yb)F_4$ and (b) $NaY(2\%Er)F_4$ NPs. Red solid lines represent the expected high temperature extrapolation of the Curie-Weiss linear behavior

of 980 nm photons. In Fig.2(a), the emission spectra correspond to the transitions from the excited levels $^2H_{11/2}$, $^4S_{3/2}$, and $^4F_{9/2}$ to the ground state $^4I_{15/2}$, which are responsible for the green light emission (∼520 and ∼550 nm) and the red one (∼670 nm), respectively. All these emissions are attributed to transitions within the J-multiplet of the Er^{3+} ions [3]. One can observe that the intensity of the green emission (500-580 nm) is lower than that of the red one (620-700 nm). This effect was attributed to a particle size dependence, where the intensity of the red band emission increases with the larger size of the particles [17]. In our case, as shown in Fig. 1 for the β-phase, we are dealing with NPs sizes of about 200 nm. Similar results were reported by Gao *et al.* for $NaY(Yb/Er)F_4$ NPs [11]. In Fig 2(b) for $NaY(30\%Yb/0.5\%Tm)F_4$ NPs, the observed emission bands at ∼451 nm and ∼477 nm represent the blue emission ($^1D_2$-$^3F_4$, $^1G_4$-$^3H_6$), and at ∼647 nm and ∼697 nm represent the red emission ($^1G_4$-$^3F_4$, and $^3F_3$-$^3H_6$). In these cases, the emitting states are attributed to transitions within the J-multiplet of the Tm^{3+} ions [3].

In order to confirm the presence and oxidation state of the dopant rare-earths ions (Er^{3+} and Yb^{3+}) we have performed *dc*-magnetic susceptibility and ESR

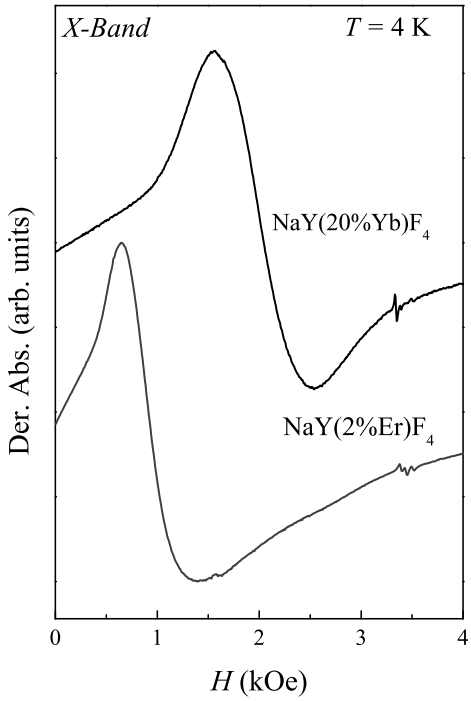

Figure 4: ESR spectra for $NaY(20\%Yb)F_4$ and $NaY(2\%Er)F_4$ NPs.

measurements in single doped $NaY(20\%Yb)F_4$ and $NaY(2\%Er)F_4$ NPs. It is shown in Fig. 3 that the temperature dependence of the magnetic susceptibility for $NaY(20\%Yb)F_4$ and $NaY(2\%Er)F_4$ NPs present a Curie-Weiss like behavior, corresponding to oxidation states of Yb^{3+} ($4f^{13}$, $J = 7/2$) and Er^{3+} ($4f^{11}$, $J = 15/2$) ions. The measured magnetic susceptibility curves for temperatures above ∼180 K was fitted to the Curie-Weiss law,

$$\chi = \chi_0 + C/(T - \Theta_{CW}). \quad (1)$$

The first term, χ_0, on the right side of eq.1 represents the diamagnetic contribution, while the second term corresponds to the paramagnetic one, where $C = x\mu^2/8$ is the Curie-Weiss constant, x is the dopant concentration, μ is the effective magnetic moment of the dopant rare-earth ions, and Θ_{CW} is the Curie-Weiss temperature. From the best fits, we obtained the concentrations of ∼17% of Yb^{3+} and ∼2.5% of Er^{3+}. These values are in reasonable agreement with the nominal concentrations of 20% and 2% used for Yb and Er, respectively. It is worth mentioning that, at low temperatures, the magnetic susceptibility of the trivalent dopant rare-earth ions might be affected by the crystal electric field of the $NaYF_4$ lattice. This effect can be better visualized in Fig. 3 by taking the inverse of the magnetic susceptibility, after subtracting the diamagnetic term, $(\chi - \chi_0)^{-1}$, as a function of temperature. A represen-

tative line of the expected high temperature extrapolation of the Curie-Weiss linear behavior is also displayed in Fig. 3. Considering the slope values of the representative lines, which intersect at zero of the coordinate axes, for both NaY(20%Yb)F_4 and NaY(2%Er)F_4 NPs we obtained concentrations of ∼14 % of Yb and ∼2.3 % of Er, respectively. These concentration values are close to the values obtained from the best fits of the measured $\chi(T)$ curves for temperatures above ∼180 K as described above. One can notice that $(\chi - \chi_0)^{-1}$ starts to deviate significantly at temperatures of the order of 250 K. A detailed and proper study regarding the crystal field effects in our NPs is not feasible at this point due to the presence of cubic and hexagonal phases in our NPs.

Finally, we show in Figure 4 the X-Band ESR spectra at 4 K for the single rare-earth doped NaY(20%Yb)F_4 and NaY(2%Er)F_4 NPs. These spectra correspond to the ESR ground state powder spectra of the Yb^{3+} and Er^{3+} localized magnetic moments diluted in $NaYF_4$. The broadening of the spectra toward higher magnetic fields is due to the anisotropy of the ground state g-values of these rare-earths. These results, together with those of magnetic susceptibility, confirm the trivalent oxidation state for these rare-earths, Yb^{3+} and Er^{3+}.

4 CONCLUSION

In summary, we have observed upconversion emissions in the visible spectral range of co-doped NaY(20%Yb/2%Er)F_4 and NaY(30%Yb/0.5%Er)F_4 NPs. These synthesized NPs present the existence of two phases (α cubic- and β hexagonal-phase). Magnetization and ESR measurements were crucial to confirm that the trivalent rare-earth ions are indeed incorporated into the $NaYF_4$ NPs and are responsible for the light upconversion mechanism observed in these systems.

5 ACKNOWLEDGMENTS

This work has been supported by FAPESP, CAPES and CNPQ agencies of Brazil. The TEM data were acquired in the LME/LNNano at the Brazilian Synchrotron Light Laboratory (LNLS).

REFERENCES

[1] R. Scheps, Prog. Quant. Electron. 20, 271, 1996.
[2] B.E. Cohen, Nature 467, 407, 2010.
[3] F. Auzel, Chem. Rev. 104, 139-173, 2004.
[4] J.F. Suyver, A. Aebischer, D. Biner, P. Gerner, J. Grimm, S. Heer, K.W. Krämer, C. Reinhard, H.U. Güdel, Optical Materials 27, 1111, 2005.
[5] F. Wang and X. Liu, Chem. Soc. Rev. 38, 976, 2009.
[6] K. Krämer, D. Biner, G. Frei, H. Güdel, M. Hehlen, and S. Lüthi, Chem. Mater. 2004, 16, 12441251
[7] F. Wang and X.G. Liu, J. Am. Chem. Soc. 130, 5642, 2008.
[8] G. Chen, T.Y. Ohulchanskyy, R. Kumar, H. Ågren, and P.N. Prasad, ACS Nano 4, 3163, 2010.
[9] J.F. Suyver, J. Grimm, M.K. van Veen, D. Biner, K.W. Krämer, H.U. Güdel, Journal of Luminescence 117, 1-12, 2006.
[10] X. Ye, J.E. Collins, Y. Kang, J. Chen, D.T.N. Chen, A.G. Yodh, and C.B. Murray, Proceeding of the National Academy of Science of the United States of America 107, 22430, 2010.
[11] D. Gao, X. Zhang, and W. Gao, J. Appl. Phys. 111, 033505, 2012.
[12] G. Wang, Q. Peng, and Y. LI, Accounts of Chemical Research 44, 322, 2011.
[13] Y.-F. Wang, L.-D. Sun, J.-W. Xiao, W. Feng, J.-C. Zhou, J. Shen, and C.-H. Yan, Chem. Eur. J. 18, 5558, 2012.
[14] J.-C. Boyer J.-C., F. Vetrone, L.A. Cuccia, and J.A. Capobianco, J. Am. Chem. Soc. 128, 7444, 2006.
[15] H.-X. Mai, Y.-W. Zhang, R. Si, Z.-G. Yan, L.-D. Sun, L.-P. You, and C.-H. Yan, J. Am. Chem. Soc. 128, 6426, 2006.
[16] J.E. Roberts, J. Am. Chem. Soc. 83, 1087, 1961.
[17] S. Schietinger, L. Menezes, B. Lauritzen, and O. Benson, Nano Lett. 9, 6, 2009.